Optical Engineering

OpticalEngineering.SPIEDigitalLibrary.org

Versatile four-axis gonioreflectometer for bidirectional reflectance distribution function measurements on anisotropic material surfaces

Hongsong Li
Meng Chen
Chenyang Deng
Ningfang Liao
Zhi Rao

SPIE.

Hongsong Li, Meng Chen, Chenyang Deng, Ningfang Liao, Zhi Rao, "Versatile four-axis gonioreflectometer for bidirectional reflectance distribution function measurements on anisotropic material surfaces," *Opt. Eng.* **58**(12), 124106 (2019), doi: 10.1117/1.OE.58.12.124106.

Versatile four-axis gonioreflectometer for bidirectional reflectance distribution function measurements on anisotropic material surfaces

Hongsong Li,[a,*] Meng Chen,[b] Chenyang Deng,[c] Ningfang Liao,[c] and Zhi Rao[a]
[a]Beijing Institute of Technology, School of Computer Science and Technology, Key Laboratory of Digital Performance and Simulation Technology, Beijing, China
[b]P & G Technologies (Beijing) Ltd, Beijing, China
[c]Beijing Institute of Technology, School of Optoelectronics, Key Laboratory of Photoelectronic Imaging Technology and System, Ministry of Education of China, Beijing, China

Abstract. The bidirectional reflectance distribution function (BRDF) data are essential for analyzing and modeling the material appearance of anisotropic surfaces. In order to acquire four-dimensional BRDF on the anisotropic material surfaces, a four-axis gonioreflectometer was designed and implemented. The instrument consists of a collimated, broadband light source, a four-axis rotation mechanism, a spectroradiometer, and a control system. The instrument is able to carry out spectral BRDF measurements over most of the incident and reflection hemispheres and the entire visible spectrum. One thousand twenty-four samples are obtained over the spectral range of 380 to 760 nm. The angular resolution of the BRDF measurement is <0.1 deg with good repeatability. A relative calibration method was adopted to obtain the absolute values of BRDFs. Various scanning schemes can be carried out by the instrument to scan the designated angular domains, enabling the instrument to capture material appearance with strong, distinctive anisotropic highlights and translucency. The obtained BRDF data of a textile sample demonstrate the instrument capability of capturing complex light scattering behaviors, including off-specular reflection peaks, off-plane reflection peaks, and backscattering. The designers of novel material appearance and computer graphics community will benefit from this work. [DOI: 10.1117/1.OE.58.12.124106]

Keywords: bidirectional reflectance distribution function measurement; anisotropic surface; appearance capture; instrument design; reflectometry.

Paper 191305 received Sep. 17, 2019; accepted for publication Dec. 9, 2019; published online Dec. 27, 2019.

1 Introduction

Appearance capture techniques provide quantitative, detailed representations of material appearance to help us understand and simulate the visual world around us.[1] The bidirectional reflectance distribution function (BRDF) is the most commonly used representation of material appearance, which is defined as the ratio of the radiance dL_r reflected from a surface in the direction (θ_r, ϕ_r) to the irradiance dE_i onto the surface from the direction (θ_i, ϕ_i):[2]

$$f_r(\theta_i, \varphi_i; \theta_r, \varphi_r) = \frac{dL_r(\theta_i, \varphi_i; \theta_r, \varphi_r)}{dE_i(\theta_i, \varphi_i)}, \quad (1)$$

where θ_i and ϕ_i are the zenith and azimuthal angles of the irradiance and θ_r and ϕ_r are the zenith and azimuthal angles of the reflected radiance.

In recent years, studying the appearance of anisotropic material surfaces has attracted more attention. One example of anisotropic material is fibrous material, including textiles,[3] hair,[4] wood,[5] and fur.[6] The microscopic fiber structures of these materials scatter the incident light on both microscale and macroscale, creating strong, distinctive anisotropic highlights and translucency,[7] as shown in Fig. 1(a). Another example of anisotropic material is metamaterial with nanometric scale structures. Since the direction and the wavelength of the reflected light from a metamaterial can be controlled by the geometric configuration of its nanometric scale structures, it can be used to design and fabricate novel appearances,[8] as shown in Fig. 1(b). To characterize the appearances of these anisotropic materials, a versatile BRDF measurement instrument is needed. Such a measurement instrument is required to carry out BRDF measurements that cover most of the incident and reflection hemispheres and the entire visible wavelength, in order to reveal the complex variations of BRDF with the angles and the wavelengths. To evaluate anisotropic materials with a wide range of specularity and anisotropy, the instrument is required to be able to sample the designated angular domains with given sampling density. The instrument also needs to be extensible so that, with slight modification, the instrument can measure other appearance representations, such as bidirectional texture function (BTF).[9]

To meet these demands, a four-axis spectral gonioreflectometer is proposed. The instrument acquires reflectance data over four angular dimensions and the spectral dimension of BRDF with flexible scanning schemes. The four-dimensional (4-D) BRDF obtained with this instrument reveals the light scattering behaviors of anisotropic materials. Compared with the other appearance measurement instruments, the proposed instrument prevails in its broadband capability, large angular range, compactness, and extensibility.

2 Related Works

Since the 1980s, numerous BRDF measurement instruments have been proposed. A simple way to categorize the

*Address all correspondence to Hongsong Li, E-mail: lihongsong@bit.edu.cn

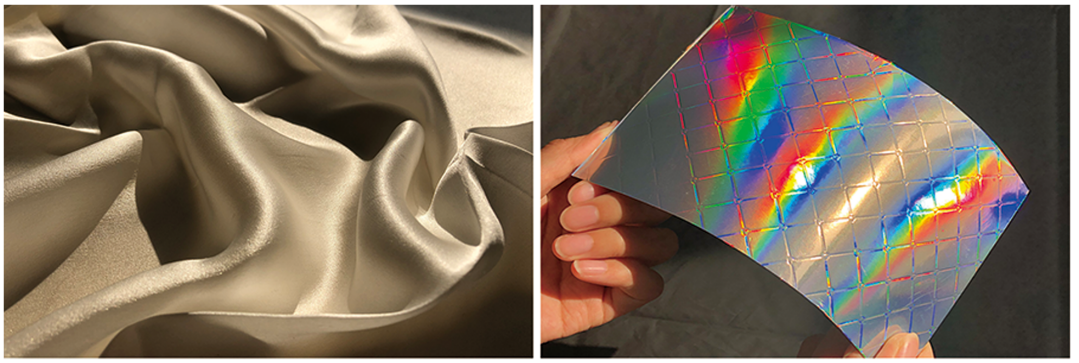

(a) (b)

Fig. 1 Examples of anisotropic material surfaces: (a) silk and (b) metamaterial.

gonioreflectometer is based on its choice of detector and its number of degrees of rotational freedom. The different choices lead to different spectral range, angular range, signal-to-noise ratio, and acquisition time of BRDF measurements.

The gonioreflectometer equipped with a radiometer or spectroradiometer as the detector is the classic setup. This class of the gonioreflectometers varies the incident and reflection angles with an optomechanical device.[10] Among this class of instruments, only a few are able to measure 4-D BRDF of anisotropic surfaces. White et al. proposed a four-axis gonioreflectometer with two-step motors to rotate the light source, one to rotate the detector, and one to rotate the sample holder.[11] Rabal et al. built a goniospectrophotometer that includes a movable spectroradiometer and a sample holder with three degrees of rotational freedom.[12] For this setup, it takes a long time (hours) to sample all the angles (in thousands), which is considered to be its major drawback. However, these detectors enable these instruments to capture accurate spectral reflectance data with a high dynamic range. And the motor-driven turntables make it easier to implement geometric calibration and to estimate the measurement uncertainty in angles.

The gonioreflectometers equipped with an imaging device as a detector are called the image-based BRDF measurement instruments. An imaging device can be considered as a detector array so that it captures multiple reflectance signals in one snapshot. With the help of the special optics, this class of gonioreflectometers accomplishes higher acquisition efficiency. Ward was the first to measure anisotropic BRDF with an imaging device.[13] With the help of a hemispherical mirror, a portion of the reflection hemisphere above the sample surface was sampled simultaneously. By pivoting the illumination direction, various θ_i and ϕ_i were sampled. Thus, among the four angles of the anisotropic BRDF, only two angles were sampled with the mechanical scan. A similar approach was further developed and more special optics were adopted, including a concave parabolic mirror (by Dana et al.),[9] an ellipsoidal mirror (by Mukaigawa et al.),[14] and a rotationally symmetric free-form mirror surface (by Ghosh et al.).[15] On the other hand, the known geometry of the sample surfaces can also help reduce the total number of sampling angles. Lu et al. measured the anisotropic BRDF of velvet by wrapping several strips of velvet samples around a cylinder with several different tangential directions.[16] Each image of the sample surface taken with this setup provided two-dimensional (2-D) samples in the 4-D angular domain of the BRDF. Ngan et al. implemented a similar approach to study anisotropic material such as satin and brushed aluminum.[17] Although the image-based measurement is more efficient in the data acquisition process, most of the imaging devices are incapable of accurate spectral measurement and offer only a limited dynamic range. The system calibration and the data processing of the obtained image data are nontrivial tasks too.

Some appearance capture devices capture both the BRDF and the BTF. Since the BTF has two more spatial dimensions than the BRDF, the BTF measurement devices, in general, include the special optics, the imaging devices, and the multiaxis mechanical scanning devices.[18–22] Some BTF measurement instruments can also capture 4-D BRDF since the BRDF can be considered as a subset of the BTF.

3 Instrument Design

An overview of the system design is shown in Fig. 2. We expect that the instrument design would be extensible so that more appearance representations, such as BTF and bidirectional transmission distribution function (BTDF), can be measured with the same setup in the future. For that reason, the detector of the proposed instrument is set to a fixed position, as shown in Fig. 2. In this work, we adopted a spectroradiometer and other categories of detectors that will be included in the future.

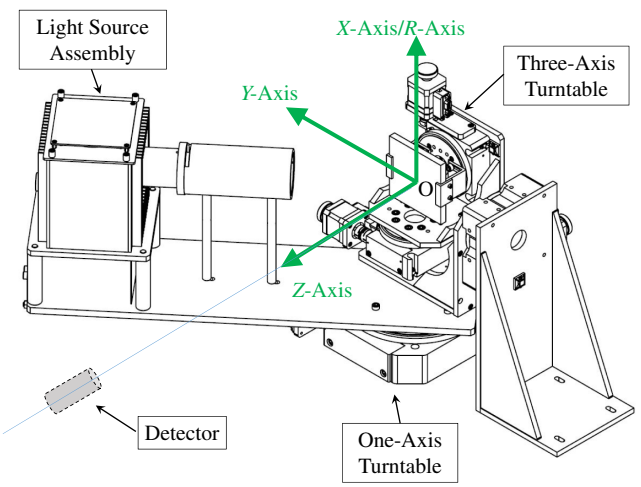

Fig. 2 Overview of the system design.

3.1 *Rotation Mechanism*

The rotation mechanism of the proposed instrument includes a one-axis motor-driven turntable driving the light source arm and a three-axis motor-driven turntable system acting as the sample holder. The one-axis turntable was installed on an optical table. A light source arm, which is a rectangular aluminum rail, was fixed on top of the turntable so that the arm can be rotated horizontally. The entire light source assembly then was installed on the light source arm. The three-axis turntable system was fixed beside the one-axis turntable, which includes two 100-mm diameter turntables and one 200-mm diameter turntable. The three rotational axes of these turntables are intersected on one point O, as shown in Fig. 2.

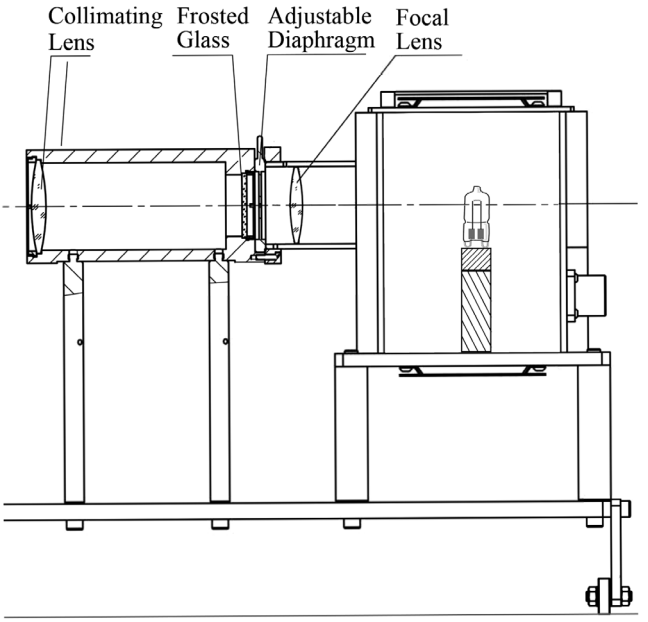

Fig. 3 The side view of the light source assembly.

A coordinate then can be defined based on point O and all the three rotational axes. The coordinate is then called the instrument coordinate.

The rotational axis of the one-axis turntable, which is called *R* axis, was aligned with *X* axis. Thus, point O is the intersection point of all four rotational axes and is then considered as the center of the sample surface for BRDF measurements. A sample holder was installed on the *Z* axis turntable that holds the sample with a clamping mechanism. The clamping mechanism was designed to guarantee that the sample surface intersects with point O and orients toward *Z* axis. In theory, any combination of the incident and reflection directions for BRDF measurements can be achieved by rotating the four turntables. The actual ranges of the rotational axes are given in Sec. 4.

3.2 *Light Source*

To provide ample coverage, a tungsten lamp with a spectral range of 300 to 2500 nm is chosen as the main light source. The light source assembly includes the tungsten lamp and a collimating optical system, as shown in Fig. 3. The tungsten lamp with housing was installed at the right end. The tungsten lamp is equipped with a focal lens that focuses the light onto a frosted glass through an adjustable diaphragm that blocks off the stray light. A collimating lens, which was installed at the left end, converts the light beam into a collimated light beam.

The diameter of the beam generated by this light source is ~60 mm. We examined the uniformity of the illuminated area with a camera by illuminating a polytetrafluoroethylene (PTFE) panel with the light source. The captured image showed that the illumination of the beam has less than 3% variation over 90% of the illuminated area, as shown in Figs. 4(a) and 4(b). The pixel values of the captured image were normalized by its maximum to illustrate the intensity distribution of the illuminated area.

The luminous flux of the light source is ~9000 lm. The illumination is required to be stable for a long period since the measurement process could take hours. To do so, a light source power supply was chosen to provide a stable output current with <0.1% fluctuation.

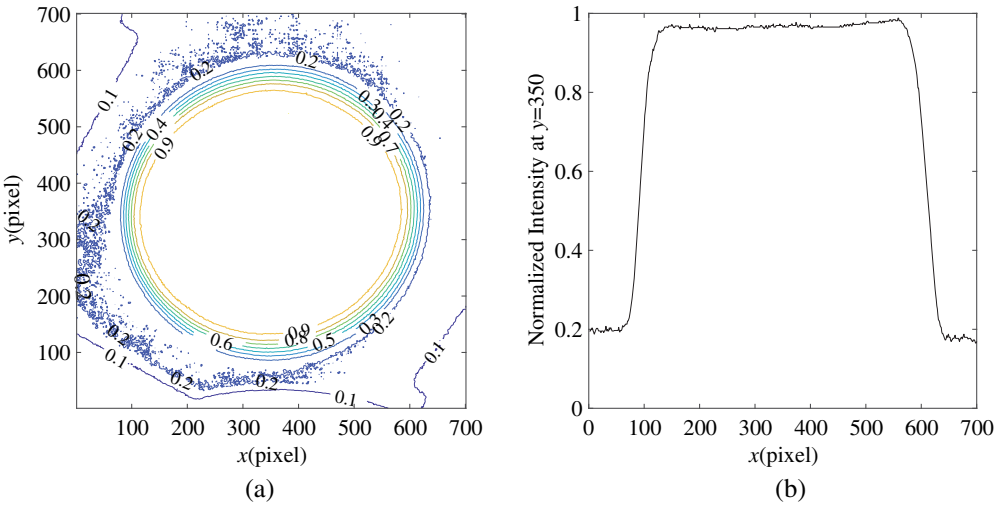

Fig. 4 Uniformity of the illuminated area by the light source: (a) contour of the light intensity and (b) normalized light intensity distribution at $y = 350$.

3.3 *Detector*

A high resolution, high dynamic range spectroradiometer was chosen for spectral BRDF measurement. The detector was aligned with the Z axis and pointing to point O. The A/D digit of the spectroradiometer is 16 bits with 1000:1 S/N ratio. In addition, it is equipped with a thermoelectric cooling unit that can reach −40°C below room temperature. This cooling unit allows the spectroradiometer to have an exposure time ranging from 8 ms to 15 min with a low level of thermal noise. The spectral range of the spectroradiometer is 380 to 760 nm with 1024 spectral samples and 0.82 to 3.3 nm spectral resolution. To examine the spectral accuracy, we measured the spectrum of a high pressure mercury lamp for reference. The high-pressure mercury lamps have prominent characteristic peaks in their output spectrum at 435.8 and 546.1 nm. The measured spectrum agreed with the characteristic peaks with less than 1 nm error.

An optical fiber probe is used to transmit the incident light into the spectroradiometer. This optical fiber probe provides us flexibility to position the detector.

During instrument alignment, an LED light source was connected to the optical fiber probe and converted the probe into a projective light source. The light source projected a light spot on the sample surface, which was used to indicate the sampling area of the detector. This feature helps to determine the maximum reflection angle of the instrument, which is ∼81 deg.

3.4 *Control System*

A computer is used to control the rotational mechanism and the spectroradiometer through a motor controller and the control unit of the spectroradiometer, respectively. A control software was developed to rotate the four turntables according to the given scanning schemes and to control the data acquisition of the spectroradiometer. The software enables automatic sampling of thousands of angular combinations sequentially. In addition, the software monitors the signal of the spectroradiometer and adjusts the exposure time based on the signal level to prevent overexposure or underexposure.

4 Implementation and Calibration of the Gonioreflectometer

The finished instrument is shown in Fig. 5. The four axes of the turntables were carefully aligned to guarantee that all the axes intersect point O. The optical fiber probe of the spectroradiometer was aligned to Z axis. Before system integration, the illumination beam of the light source was aligned separately to make the optical axis of the illumination beam intersect point O too.

A beam-splitting cube was added between the sample and the optical fiber probe. It allows one more detector to share the reflection light path with the spectroradiometer.

We define the rotational angles of X axis, Y axis, and Z axis as θ_X, θ_Y, and θ_Z. Their counterclockwise direction is defined as the positive direction. The range of θ_X is −180 deg to 180 deg; the range of θ_Y is −90 deg to 90 deg; and the range of θ_Z is −180 deg to 180 deg. We define the rotational angles of R axis as θ_R and its clockwise direction as the positive direction. Since the light source arm can be blocked by the detector, the range of θ_R is 17 deg to 180 deg.

The angular accuracy and repeatability of the turntables were tested by rotating each motor with a random angle on either clockwise or anticlockwise direction for 1000 times. Then, we let the motor return to its initial position. It shows that each motor has less than 0.1 deg shift after 1000 rotations. The main source of this error is the backlash in the lead screw of the turntables.

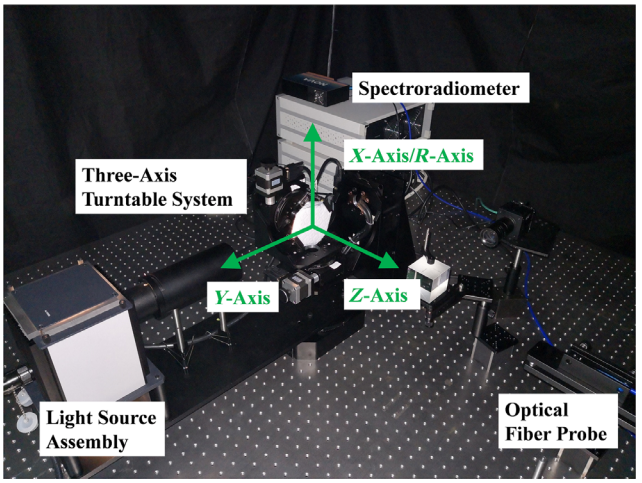

Fig. 5 The finished gonioreflectometer.

After the system alignment, we implemented a relative BRDF measurement method, which is similar to the work of Li et al.[23] A reference sample, which is a 100 mm × 100 mm flat PTFE panel, was mounted on the sample holder to obtain the reference spectroradiometric reading $V_{r,\mathrm{PTFE}}(\lambda)$ before the BRDF measurements. The incident angle θ_i for reference sample measurement was 0 deg and the reflection angle θ_r was 20 deg. This measured spectroradiometric reading corresponds to a known BRDF value derived from the unique reflection properties of PTFE, which are spectrally neutral (<1% variation over the visible spectrum), highly reflective (99% total reflectance), and close to Lambertian at normal incidence. Here, we estimate that its spectral BRDFs over the visible wavelength are approximately $f_{r,\mathrm{PTFE}} \approx 0.99/\pi \approx 0.315$ over the visible wavelength range. Then, the BRDFs of the sample surface can be estimated by

$$f_r(\lambda,\theta_i,f_i,\theta_r,f_r) = \frac{V_{r,\mathrm{sample}}(\lambda,\theta_i,f_i,\theta_r,f_r) - V_{\mathrm{bkg}}(\lambda)}{V_{r,\mathrm{PTFE}}(\lambda) - V_{\mathrm{bkg}}(\lambda)} \cdot \frac{f_{r,\mathrm{PTFE}}(\lambda)}{\cos(\theta_i)}, \tag{2}$$

where $V_{r,\mathrm{sample}}(\lambda,\theta_i,\phi_i,\theta_r,\phi_r)$ is the spectroradiometric reading of the reflected radiance from the sample surface for each angular configuration; $V_{\mathrm{bkg}}(\lambda)$ is the spectroradiometric reading of the background signal.

To deal with the high dynamic range of BRDF data, $V_{r,\mathrm{PTFE}}(\lambda)$ and $V_{\mathrm{bkg}}(\lambda)$ were captured at a series of selected exposure times, ranging from 10 ms to 2 s. During the BRDF measurements, the control software automatically adjusted the exposure time of the spectroradiometer among these selected exposure times, to prevent over-/underexposure. For each captured $V_{r,\mathrm{sample}}(\lambda,\theta_i,\phi_i,\theta_r,\phi_r)$, we also recorded its exposure time for later data processing. Then $V_{r,\mathrm{PTFE}}(\lambda)$ and $V_{\mathrm{bkg}}(\lambda)$ corresponding to this recorded exposure time were extracted.

In order to validate the proposed instrument and the relative BRDF measurement method, the BRDFs of the PTFE

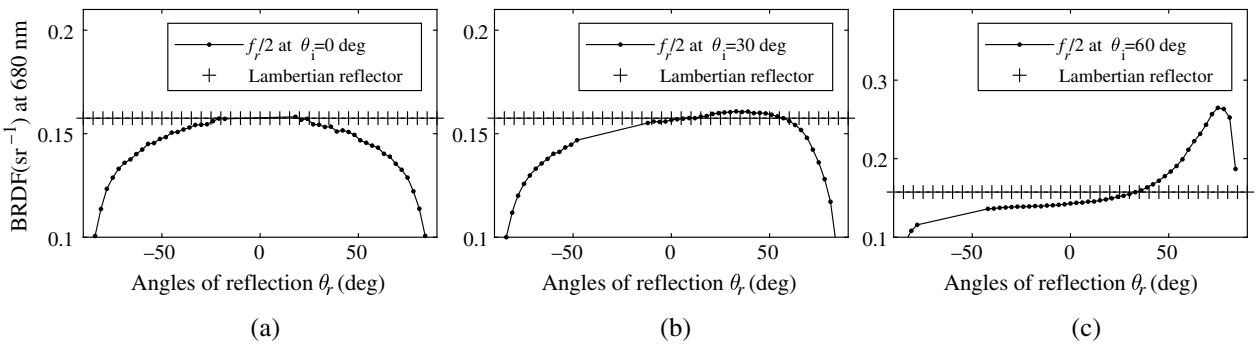

Fig. 6 Incidence-plane BRDFs of PTFE reference sample at 680-nm wavelength and various incidence angles: (a) $\theta_i = 0$ deg, (b) $\theta_i = 30$ deg, and (c) $\theta_i = 60$ deg.

reference sample on the incidence plane were measured at $\theta_i = 0$ deg, 30 deg, and 60 deg. The obtained BRDF data at 680-nm wavelength are plotted in Fig. 6. We compare the obtained BRDF data with the incidence-plane BRDF data published by Bhandari et al.,[24] which were measured with collimated, unpolarized illumination at the same wavelength and the same incidence angles. In their work, the unpolarized BRDF data were divided by 2 to compare with the polarized BRDF data, and a horizontal line of symbols "+" at $f_r = 1/2\pi$ were added to each plot to illustrate the BRDF of an ideal Lambertian reflector. Our data were plotted in the same way. The angular distribution of BRDF obtained by the proposed instrument matches well with the published BRDF data. Our data show a slightly lower magnitude since we assume that the BRDF of PTFE reference sample $f_{r,\mathrm{PTFE}} \approx 0.315$ at $\theta_i = 0$ deg and $\theta_r = 20$ deg, whereas the published BRDF data have the same value as the Lambertian reflector at $\theta_i = 0$ deg and $\theta_r \approx 50$ deg. In addition, our BRDF data have a lower magnitude at large angles of reflection ($\theta_r > 80$ deg) than the published BRDF data. At large angles of reflection, the projected area (or sampling area) of the detector aperture exceeds the illuminated area on the sample surface or the entire sample surface, leading to lower reflection signals. Although reducing the detector aperture improves the measurement accuracy, it has a negative effect on the signal-to-noise ratio. In this work, we are trading the accuracy for better signal-to-noise ratio. The difference in the surface finish of the PTFE reference sample and the Spectralon sample used for the published data is another possible source of the differences in the two datasets.

5 4-D Scanning Scheme Design

For the isotropic surfaces, three-dimensional (3-D) scanning schemes that sample θ_i, θ_r and ϕ_I, $-\phi_r$ well characterize the light scattering behaviors of the target surface, and the symmetric nature of the surface allows sampling only half of the reflection hemisphere. For the anisotropic surfaces, all four angles need to be sampled. We propose a 4-D scanning scheme to determine the sampling directions over the incident and reflection hemisphere.

5.1 *4-D Sampling Directions in the Sample Coordinate*

We assume that the material surface is flat, anisotropic, and has two orthogonal tangential directions in its microscale structure. And the surface is symmetric at both sides of each of the tangential directions. In this case, only one-fourth of the incident hemisphere needs to be sampled. Altogether 16 reflection directions with uniform intervals in θ_i and ϕ_i were chosen, where $\theta_i = 10$ deg, 30 deg, 50 deg, 70 deg and $\phi_i = 0$ deg, 30 deg, 60 deg, 90 deg. For each combination of θ_i and ϕ_i, we initially chose 400 sampling directions over the reflection hemisphere. It was done by sampling directions on a regular grid on the unit square, and then mapping these positions to the unit reflection hemisphere with a transformation that produces a uniform distribution in solid angle.[25] Among the 400 sampling directions, those positions over the limit of the reflection angles ($\theta_r > 80$ deg) and too close to the incident directions (within 17 deg) were excluded. After that, approximately 300 sampling directions for each incident direction were obtained. The total number of sampling directions of this 4-D sampling scheme was 5184. The sampling directions over the incident and reflection hemisphere are shown in Fig. 7. The red color vectors represent the incident directions, and the blue color dots represent the sampling directions over the reflection hemisphere.

The density of the sampling directions over the incident and reflection hemisphere can be adjusted here so that various scanning schemes can be produced with this approach.

5.2 *4-D Sampling Angles in the Instrument Coordinate*

After a complete 4-D sampling scheme was obtained in the sample coordinate, we converted these sampling directions to the instrument coordinate. We first mapped the sample coordinate onto the instrument coordinate, where the red color represents the sample coordinate and green color represents the instrument coordinate, as shown in Fig. 7. In the sample coordinate, $\vec{\mathbf{L}}$ is the illumination direction vector, $\vec{\mathbf{N}}$ is the surface normal, and $\vec{\mathbf{V}}$ is the viewing direction vector. And we have $\vec{\mathbf{L}} = [\sin\theta_i \cos\phi_i \sin\theta_i \sin\phi_i \cos\theta_i]$, $\vec{\mathbf{V}} = [\sin\theta_r \cos\phi_r \sin\theta_r \sin\phi_r \cos\theta_r]$, and $\vec{\mathbf{N}} = z = [0\,0\,1]$. In the instrument coordinate, X axis and Y axis turntables reorient of the surface normal $\vec{\mathbf{N}}'$; Z axis turntable makes the sample rotate around $\vec{\mathbf{N}}'$; and R axis turntable varies the incident direction $\vec{\mathbf{L}}'$. We have $\vec{\mathbf{L}}' = [0 \sin\theta_R \cos\theta_R]$ and $\vec{\mathbf{N}}' = [\cos\theta_X \sin\theta_Y - \sin\theta_X \cos\theta_X \cos\theta_Y]$. Since the detector is in a fixed direction, the viewing direction vector in the instrument coordinate $\vec{\mathbf{V}}'$ is always [0 0 1].

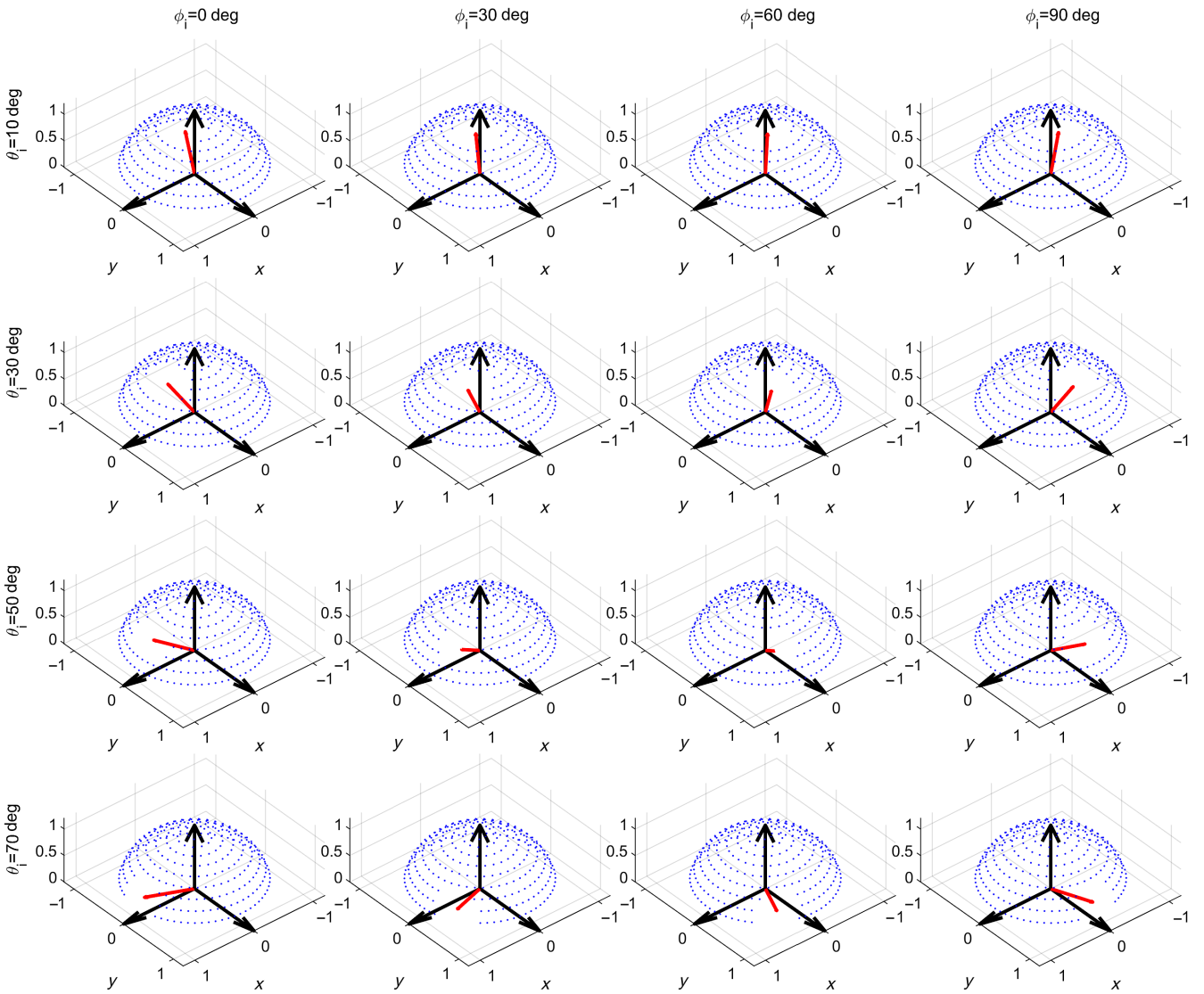

Fig. 7 The BRDF sampling directions over the incident and reflection hemisphere.

From Fig. 8, we also have

$$\cos\theta_R = \|\vec{\mathbf{L}}\cdot\vec{\mathbf{V}}\|, \tag{3}$$

$$\cos\theta_i = \|\vec{\mathbf{L}}\cdot\vec{\mathbf{N}}\| = \|\vec{\mathbf{L}}'\cdot\vec{\mathbf{N}}'\|, \tag{4}$$

$$\cos\theta_r = \|\vec{\mathbf{V}}\cdot\vec{\mathbf{N}}\| = \|\vec{\mathbf{V}}'\cdot\vec{\mathbf{N}}'\|. \tag{5}$$

From Eqs. (3)–(5), we derive that

$$\theta_R = \text{arc}\cos(\|\vec{\mathbf{L}}\cdot\vec{\mathbf{V}}\|), 0 < q_R < 180 \text{ deg}, \tag{6}$$

$$\theta_X = \text{arc}\sin\left(\frac{\cos\theta_r\cos\theta_R - \cos\theta_i}{\sin\theta_R}\right), \quad -90\,\text{deg} < q_X < 90\,\text{deg}. \tag{7}$$

$$\theta_Y = \text{arc}\cos\left(\frac{\cos\theta_r}{\cos\theta_X}\right), 0 \text{ deg} < q_Y < 180 \text{ deg}. \tag{8}$$

Since θ_Y is set to be between -90 deg and 90 deg, the obtained θ_Y by Eq. (8) was mapped from 0 deg to 180 deg to -90 deg to 90 deg, according to the value of $|\phi_i - \phi_r|$.

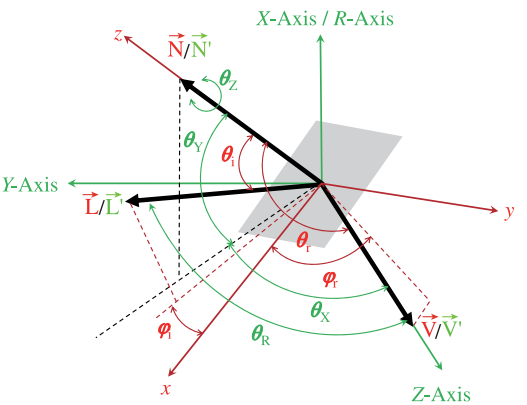

Fig. 8 Mapping the sample coordinate to the instrument coordinate.

For an anisotropic surface, θ_Z was adjusted so that x and y axes of the sample coordinate were rotated until they reach the position shown in Fig. 8. To do so, x, y, and z axes of the sample coordinate were transformed to the instrument coordinate by

$$\mathbf{R_{YXZ}} = \mathbf{R_Y R_X R_Z} = \begin{bmatrix} \cos\theta_Y \cos\theta_Z + \sin\theta_X \sin\theta_Y \sin\theta_Z & -\cos\theta_Y \sin\theta_Z + \sin\theta_X \sin\theta_Y \cos\theta_Z & \cos\theta_X \sin\theta_Y \\ \cos\theta_X \sin\theta_Z & \cos\theta_X \cos\theta_Z & -\sin\theta_X \\ -\sin\theta_Y \cos\theta_Z + \sin\theta_X \cos\theta_Y \sin\theta_Z & \sin\theta_Y \sin\theta_Z + \sin\theta_X \cos\theta_Y \cos\theta_Z & \cos\theta_X \cos\theta_Y \end{bmatrix}, \quad (9)$$

where $\mathbf{R_X}$, $\mathbf{R_Y}$, and $\mathbf{R_Z}$ are the transformation matrices of rotation around X axis, Y axis, and Z axis, respectively. After determining x, y, and z axes of the sample coordinate in the instrument coordinate, we then projected $\vec{\mathbf{L}}$ and $\vec{\mathbf{V}}$ to the plane defined by x and y axes. The angle between the projection of $\vec{\mathbf{L}}$ and x axis needs to be ϕ_i; and the angle between the projection of $\vec{\mathbf{V}}$ and x axis needs to be ϕ_r. This allowed us to determine θ_Z that meets these requirements.

The obtained angle combinations of θ_X, θ_Y, θ_Z, and θ_R are the motor control data and were used to control the turntables during data acquisition. For the 4-D sampling scheme with 5184 angular configurations, the total time for data acquisition was ~9 h. Although the total data acquisition time seems quite long, the proposed instrument acquires significantly more data samples than the similar gonioreflectometers at a faster rate.[12]

6 BRDF Data and Analysis

An anisotropic sample, which is an antistatic lining fabric made with 100% polyester, was chosen to demonstrate the capability of the proposed instrument. The sample is a purely white, plain textile and has an anisotropic, glossy appearance. Its BRDF was measured using the scanning scheme shown in Fig. 7.

6.1 *Spectral Data Processing*

We chose one angular configuration to illustrate the obtained spectral BRDF, as shown in Fig. 9. The obtained spectral signals of the background signal $V_{\text{bkg}}(\lambda)$, the reference $V_{r,\text{PTFE}}(\lambda)$, and the captured raw data $V_{r,\text{sample}}$ (λ, 70 deg, 0 deg, 78.5 deg, 177.3 deg) are compared in Fig. 9(a). The exposure time of these three spectral signals was 200 ms. And the obtained absolute BRDF values at this angular configuration were calculated by Eq. (2) and shown in Fig. 9(b). The signal level at the short wavelengths end was relatively low, which was the result of low output of the light source in the short wavelengths. The lenses also have a lower spectral transmittance at short wavelength band. As a result, the signal-to-noise ratio of the obtained spectral BRDF from 380 to 420 nm is slightly lower than the rest of the visible spectrum.

We calculated the spectral BRDFs for all 5184 angular configurations. Since the sample is pure white, the spectral distribution of these spectral BRDFs is quite similar. Thus, we chose one wavelength (550 nm) to present the angular variations of the BRDF data.

6.2 *4-D BRDF Data in One Wavelength*

For each combination of θ_i and ϕ_i, we plotted its corresponding BRDFs over the reflection hemisphere. The hemispherical distribution of BRDF was mapped to a coordinate so that its x ($x = \sin\theta_r \cos\phi_r$) and y ($y = \sin\theta_r \sin\phi_r$) coordinates represent the reflection directions while the vertical axis of the new coordinate is the magnitude of BRDFs, as shown in Fig. 10(a). This mapping method exaggerates the sampling directions with small θ_r but helps to illustrate the anisotropy of measured BRDF by providing a uniform mapping of ϕ_r. On the surface of the 3-D plot, a black curve was added to illustrate the incidence plane. Note that a section of the black curve was blocked by a reflection peak in BRDF data.

Additionally, the contours of the measured BRDFs were plotted, where x and y coordinates are from the same mapping method but the magnitude of the measured BRDF is presented as the colored contours, as shown in Fig. 10(b). In the contour plot, a black arrow was added to represent the azimuthal direction of incidence. Multiple isometric lines (dotted lines) of θ_r and ϕ_r were added, which helps to estimate the positions of the reflection peaks. For both 3-D and contour plots, the magnitude of the BRDF is presented with the same color map.

Both plots of Fig. 10 show that the reflection peaks are not symmetric about the incidence plane. It implies that the

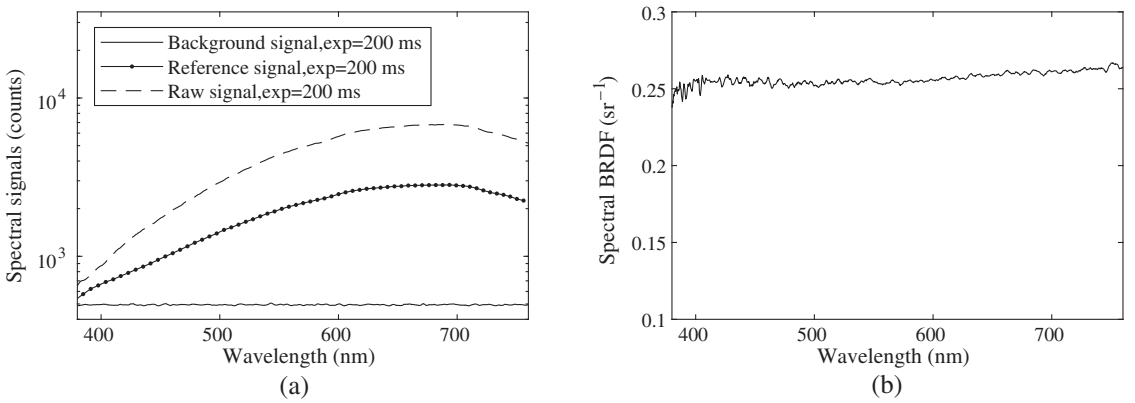

Fig. 9 Measured spectral BRDFs: (a) captured spectral signals and (b) obtained absolute BRDF at one angular configuration.

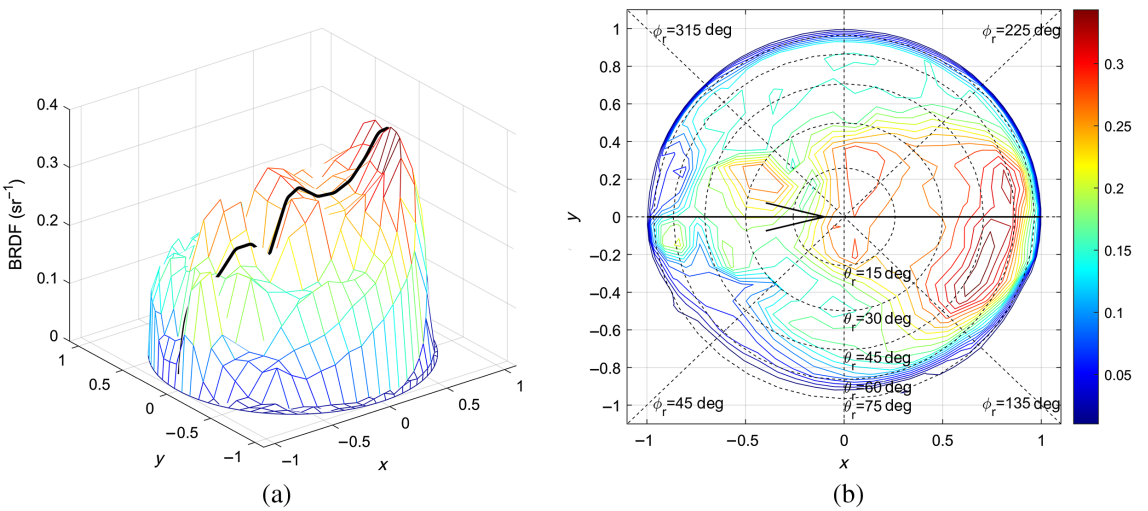

Fig. 10 Measured BRDFs at 550-nm wavelength, over the reflection hemisphere, and at $\theta_i = 30$ deg and $\phi_i = 0$ deg, illustrated with two mapping methods: (a) 3-D mapping and (b) colored contour.

incident directions are not aligned with the weave directions of the fabric. We did not intentionally align the directions of weave pattern (or the tangential directions of the fabric texture) with X-axis or Y-axis when the sample was mounted. As a result, none of the measured hemispherical BRDF distribution are symmetric about the incidence plane.

Both plots of Fig. 10 show that multiple reflection peaks can be observed from measured BRDFs.

For an incident angle at $\theta_i = 30$ deg and $\phi_i = 0$ deg, three classes of reflections peaks can be observed. The reflection peak with the maximum BRDF values is in the range of $\theta_r = 45$ deg to 60 deg and $\phi_r = 135$ deg to 200 deg, as shown in Fig. 10(b). This off-specular peak at grazing angles, which is a result of volumetric scattering, can be observed on many fibrous materials. The fibers act as curved optical fibers and redirect the incident light toward the grazing angles.[7] The second reflection peak can be observed at in the range of $\theta_r = 0$ deg to 30 deg and $\phi_r = 90$ deg to 270 deg, which is a result of first-surface reflections and back-surface reflections on the fiber surfaces. The surface of the fibers is not always parallel to the material surface, which makes the second reflection peak slight off the specular reflection direction. The rest of the reflection peaks are in the range of $\phi_r = -45$ deg to 45 deg, which are backscattering components and results of volumetric scattering. The three classes of reflection peaks were all predicted by the theoretical research of appearance modeling of fibrous materials.[7]

The 4-D BRDF data in 550-nm wavelength are presented as a 2-D matrix of 3-D BRDF plots, as shown in Fig. 11. The two dimensions of the matrix represent the zenith and the azimuthal angles of incidence θ_i and ϕ_i, which is consistent with Fig. 7. The 4-D BRDF data further revealed the correlation of the measured BRDFs and the angles.

In Fig. 11, the distribution of BRDF data varies with both θ_i and ϕ_i. None of the 3-D plots of BRDF are symmetric about the incidence plane. The off-specular peaks at grazing angles grow stronger and become more symmetric with the increase of θ_i, while the other two classes of reflection peaks diminish. However, at $\theta_i = 70$ deg, the backscattering components are not negligible. This anisotropic characteristic of BRDF makes the appearance of the fibrous material distinctive from other materials. The obtained BRDF data of an anisotropic material demonstrate the complexity of the light scattering behavior from a typical anisotropic material, which help us understand the scattering characteristics of these anisotropic materials and relate the complex highlights of these materials with the incidence and reflection angles. Therefore, the obtained BRDF data are especially valuable for developing theoretical BRDF models for these material surfaces.

7 Conclusion

In this work, we present a spectral BRDF measurement instrument. The instrument measures anisotropic BRDFs by sampling most of the incident and reflection hemispheres. To do so, a three-axis turntable system acts as a sample holder, and a one-axis turntable is used to rotate the light source on a horizontal plane. This setup provides four axes of rotation needed for sampling four angles of anisotropic BRDF. The light source is equipped with a tungsten lamp, which has a spectral range of 300 to 2500 nm. A spectroradiometer equipped with a fiber probe is used to measure the reflective spectrum of the sample surface. The spectral range of the spectroradiometer is 380 to 760 nm with 1024 spectral samples. As a result, the instrument is able to obtain spectral BRDF data in the spectral range of 380 to 760 nm with sufficient samples. A control software was developed to control the four turntables according to the input motor control data and capture the spectrum data from the spectroradiometer. A relative calibration method was implemented to obtain the absolute value of BRDF. A PTFE panel was chosen as the reference sample with known reflectance properties. To deal with the high dynamic range of the BRDF values, over-/underexposure of the spectroradiometer is detected and appropriate exposure time is then applied by the control software.

A scanning scheme design method is introduced. It allows us to sample the incident and reflection hemisphere with the chosen sampling density. Then, the sampling directions in the sample coordinate are converted to the motor control

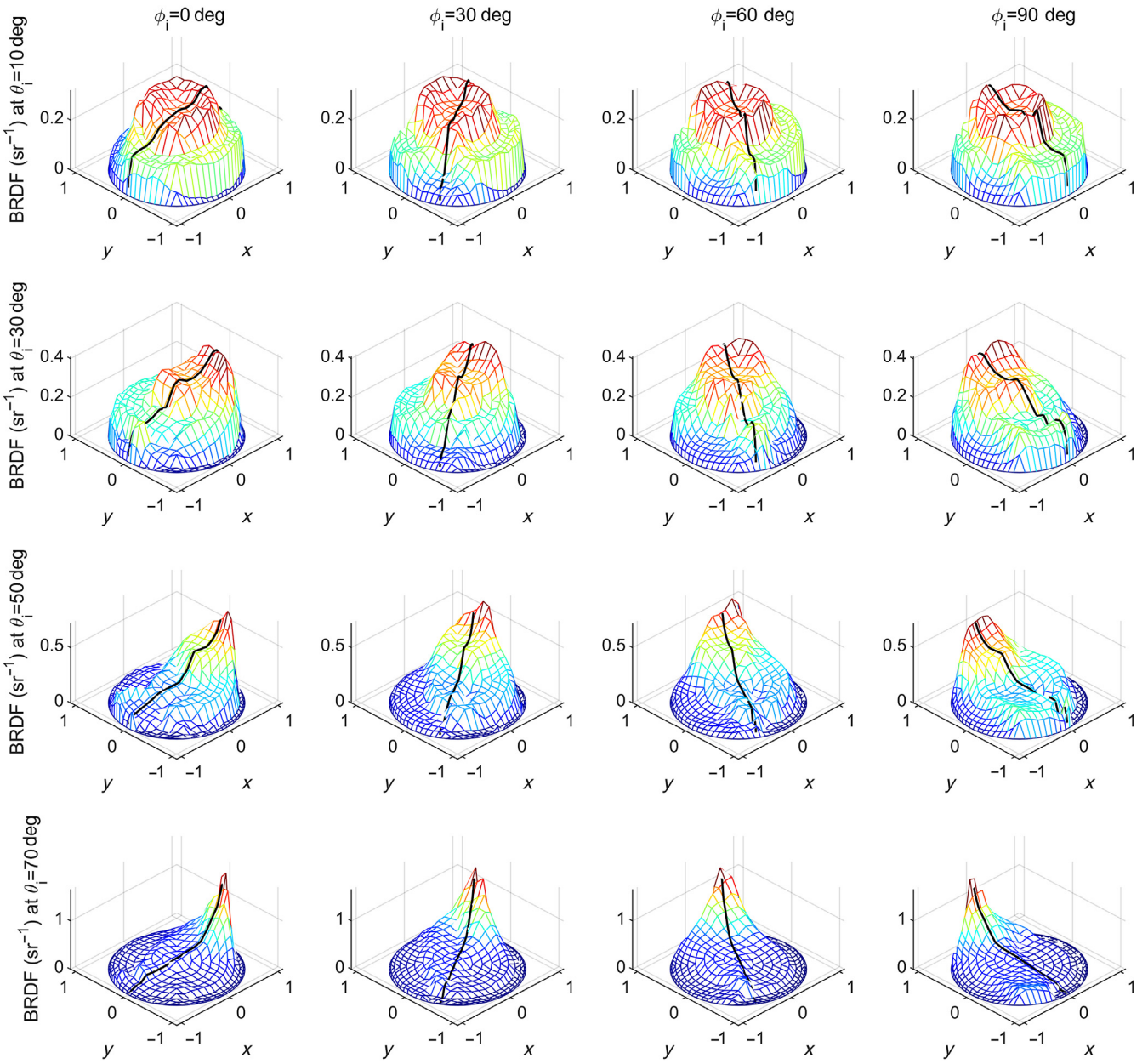

Fig. 11 Measured BRDFs at 550-nm wavelength, over the reflection hemisphere, and at various θ_i and ϕ_i.

data, which include the rotation angles of the four turntables for each sampling direction.

To demonstrate the capability of the proposed instrument, an anisotropic textile sample was chosen for BRDF measurement. A 4-D scanning scheme of 5084 sampling directions was used to control the scanning process. The obtained BRDF data reveal the multiple reflection peaks at various incidence/reflection directions, including off-specular reflection peaks, off-plane reflection peaks, and backscattering. This data is especially useful for analyzing the light scattering phenomenon of anisotropic materials with microscopic structures. With a good understanding of the microscopic structure of such material, BRDF models of these novel materials can be proposed based on the obtained BRDF data.

The proposed instrument has several limitations. First, the light source has low output intensity at certain wavebands. It causes a lower level of signal-to-noise ratio at the short wavelength end of the visible spectrum. Second, the detector blocks the light source so that a portion of the reflection hemisphere is unreachable. Third, the diameter of the beam generated by the light source limits the angular range of BRDF measurement, leading to a lower magnitude in BRDF data captured at large angles of reflection.

The extensibility of the proposed instrument allows us to acquire other types of appearance data in the future. The setup is capable of measuring BTDF by positioning the detector and the light source on opposite sides of the sample. By adding a beam-splitting cube, one more detector such as a RGB camera can share the light path of the spectroradiometer and enable BTF measurement.

Acknowledgments

This work has been supported by National Key R&D Program of China under Grant No. 2018YFB1403900 and

National Natural Science Foundation of China (NSFC) under Grant Nos. 61975012 and 60975013.

References

1. T. Weyrich et al., "Principles of appearance acquisition and representation," *Found. Trends Comput. Graphics Vision* **4**(2), 75–191 (2007).
2. F. E. Nicodemus et al., *Geometric Considerations and Nomenclature for Reflectance*, Monograph 160, National Bureau of Standards (1977).
3. S. C. Pont and J. J. Koenderink, "Split off-specular reflection and surface scattering from woven materials," *Appl. Opt.* **42**, 1526–1533 (2003).
4. S. R. Marschner et al., "Light scattering from human hair fibers," *ACM Trans. Graphics* **22**(3), 780–791 (2003).
5. S. R. Marschner et al., "Measuring and modeling the appearance of finished wood," *ACM Trans. Graphics* **24**(3), 727–734 (2005).
6. L.-Q. Yan et al., "Physically-accurate fur reflectance: modeling, measurement and rendering," *ACM Trans. Graphics* **34**(6), 1–13 (2015).
7. K Schröder, S. Zhao, and A. Zinke, "Recent advances in physically-based appearance modeling of cloth," in *Siggraph Asia 2012* (2012).
8. K. Smistrup et al., "Designing visual appearance using a structured surface," *Optica* **2**(3), 239–245 (2015).
9. K. Dana et al., "Reflectance and texture of real-world surfaces," *ACM Trans. Graphics* **18**, 1–34 (1999).
10. J. F. Murray-Coleman and A. M. Smith, "The automated measurement of BRDFs and their application to luminaire modeling," *J. Illum. Eng. Soc.* **19**(1), 87–99 (1990).
11. D. R. White et al., "Reflectometer for measuring the bidirectional reflectance of rough surfaces," *Appl. Opt.* **37**(16), 3450–3454 (1998).
12. A. M. Rabal et al., "Automatic gonio-spectrophotometer for the absolute measurement of the spectral BRDF at in- out-of-plane and retroreflection geometries," *Metrologia* **49**(3), 213–223 (2012).
13. G. J. Ward, "Measuring and modeling anisotropic reflection," *ACM Siggraph Comput. Graphics* **26**, 265–272 (1992).
14. Y. Mukaigawa, K. Sumino, and Y. Yagi, "Multiplexed illumination for measuring BRDF using an ellipsoidal mirror and a projector," *Lect. Notes Comput. Sci.* **4844**, 246–257 (2007).
15. A. Ghosh et al., "BRDF acquisition with basis illumination," in *Proc. IEEE Int. Conf. Comput. Vision*, IEEE (2007).
16. R. Lu, J. J. Koenderink, and A. M. L. Kappers, "Optical properties (bidirectional reflection distribution functions) of velvet," *Appl. Opt.* **37**, 5974–5984 (1998).
17. A. Ngan, F. Durand, and W. Matusik, "Experimental analysis of BRDF models," in *Rendering Tech.*, Springer, pp. 117–126 (2005).
18. M. Sattler, R. Sarlette, and R. Klein, "Efficient and realistic visualization of cloth," in *Rendering Tech.*, Springer, pp. 167–178 (2003).
19. K. J. Dana and J. Wang, "Device for convenient measurement of spatially varying bidirectional reflectance," *J. Opt. Soc. Am. A* **21**, 1–12 (2004).
20. J. Y. Han and K. Perlin, "Measuring bidirectional texture reflectance with a kaleidoscope," *ACM Trans. Graphics* **22**, 741–748 (2003).
21. J. Hosek et al., "Optomechanical design of a portable compact bidirectional texture function measurement instrument," *Appl. Opt.* **56**, 1183–1193 (2017).
22. J. Čáp et al., "Optomechanical design of rotary kaleidoscope for bidirectional texture function acquisition," *Appl. Opt.* **56**, 7373–7384 (2017).
23. H. Li et al., "Automated three-axis gonioreflectometer for computer graphics applications," *Opt. Eng.* **45**, 043605 (2006).
24. A. Bhandari et al., "Bidirectional reflectance distribution function of spectralon white reflectance standard illuminated by incoherent unpolarized and plane-polarized light," *Appl. Opt.* **50**(16), 2431–2442 (2011).
25. P. Shirley and K. Chiu, "Notes on adaptive quadrature on the hemisphere," Technical Report 441, Department of Computer Science, Indiana University, Bloomington, Indiana (1994).

Hongsong Li is an associate professor at School of Computer Science and Technology of Beijing Institute of Technology. He received his BS degree in optoelectronic engineering from Beijing Institute of Technology in 1994, his MS degree in engineering mechanics from Tsinghua University in 1998, and his PhD from Cornell University in 2005. His current research interests include computer graphics, computer vision, human–computer interaction, and optical engineering.

Biographies of the other authors are not available.